

Heavy ion beam probe advances from the first installation of the diagnostic on an RFP (invited)

D. R. Demers and P. J. Fimognari

Citation: *Rev. Sci. Instrum.* **83**, 10D711 (2012); doi: 10.1063/1.4731758

View online: <http://dx.doi.org/10.1063/1.4731758>

View Table of Contents: <http://rsi.aip.org/resource/1/RSINAK/v83/i10>

Published by the [American Institute of Physics](http://www.aip.org).

Additional information on *Rev. Sci. Instrum.*

Journal Homepage: <http://rsi.aip.org>

Journal Information: http://rsi.aip.org/about/about_the_journal

Top downloads: http://rsi.aip.org/features/most_downloaded

Information for Authors: <http://rsi.aip.org/authors>

ADVERTISEMENT

physicstoday

Comment on any
Physics Today article.

Physics Today / Volume 63 / Issue 7 / July 2012
Previous Article | Next Article

Measured energy in Japan
David von Seggern
(dvseg@seismo.unr.edu) University of Nevada
July 2012, page 10
DIGITAL OBJECT IDENTIFIER
<http://dx.doi.org/10.1063/PT.3.1619>

The article by Thorne Lay and Hiroo Kanamori (10D711) is an excellent review of the 1994 Chilean earthquake and the energy released. The authors used the relation for seismic energy release rather than total strain energy release. The seismic energy release is a variable that depends on friction on the fault plane. Accounting for total strain energy release would increase the earthquake energy number by orders of magnitude.

Despite the catastrophic damage potential of nuclear bombs, the forces of nature occasionally unleash much larger energy releases. Although the nuclear bombs are under our control, earthquakes, volcanic eruptions, and extreme weather events are not. However, by judicious preparation and avoidance measures, humans can significantly diminish the damage of natural events.

This article does not have any references.

Comment on this article
By the act of hitting a ball with a bat, one calculates the force energy to deliver the ball to its new location, but one must also take into account that the ball extended its energy to the struck team, which became struck by the ball as its momentum ceased and passed energy to the struck team. Therefore the parameters of the damage extend into the future when the received energy to that pushed upon, later becomes released in a new event. Perhaps calculations of one added that in, while another's calculations did not. E.M.C.
Written by Edgar Mocarvill, 14 July 2012 19:59

Heavy ion beam probe advances from the first installation of the diagnostic on an RFP (invited)^{a)}

D. R. Demers^{b)} and P. J. Fimognari

Xantho Technologies, LLC, Madison, Wisconsin 53705, USA

(Presented 8 May 2012; received 8 May 2012; accepted 5 June 2012; published online 10 July 2012)

Heavy ion beam probes have been installed on a variety of toroidal devices, but the first and only application on a reversed field pinch is the diagnostic on the Madison Symmetric Torus. Simultaneous measurements of spatially localized equilibrium potential and fluctuations of density and potential, previously inaccessible in the core of the reversed field pinch (RFP), are now attainable. These measurements reflect the unique strength of the heavy ion beam probe (HIBP) diagnostic. They will help determine the characteristics and evolution of electrostatic fluctuations and their role in transport, and determine the relation of the interior electric field and flows. Many aspects of the RFP present original challenges to HIBP operation and inference of plasma quantities. The magnetic field contributes to a number of the issues: the comparable magnitudes of the toroidal and poloidal fields and edge reversal result in highly three-dimensional beam trajectories; partial generation of the magnetic field by plasma current cause it and hence the beam trajectories to vary with time; and temporal topology and amplitude changes are common. Associated complications include strong ultraviolet radiation and elevated particle losses that can alter functionality of the electrostatic systems and generate noise on the detectors. These complexities have necessitated the development of new operation and data analysis techniques: the implementation of primary and secondary beamlines, adoption of alternative beam steering methods, development of higher precision electrostatic system models, refinement of trajectory calculations and sample volume modeling, establishment of stray particle and noise reduction methods, and formulation of alternative data analysis techniques. These innovative methods and the knowledge gained with this system are likely to translate to future HIBP operation on large scale stellarators and tokamaks. © 2012 American Institute of Physics. [<http://dx.doi.org/10.1063/1.4731758>]

I. HEAVY ION BEAM PROBE

A. Background and principles

Heavy ion beam probes (HIBP) have been installed on a wide range of toroidal configurations; a detailed description of many of the resulting operating principles, methods, and techniques has been published.¹ The first and only application on a reversed field pinch (RFP) is the diagnostic installed on the Madison Symmetric Torus (MST). Many aspects of the RFP present original challenges to HIBP operation and inference of plasma quantities. These include the dynamic multi-dimensional nature of the RFP magnetic field, small diagnostic ports, and a high flux of ultraviolet photons. Operational and diagnostic advances in response to these challenges make HIBP measurements in the core of the RFP attainable.

Simultaneous measurements of spatially localized equilibrium potential and fluctuations of density and potential in the interior of high temperature magnetically confined plasmas are the strength of the HIBP diagnostic. These measurements determine the characteristics and evolution of electrostatic fluctuations and electric field, as well as their role in

transport and flows. Application of the diagnostic on an RFP provides data that complements measurements in other magnetic configurations allowing issues to be investigated over a broad parameter space.

A basic heavy ion beam probe operates with a beam of singly charged ions (primaries). The primaries undergo electron impact ionization along their path in the plasma, resulting in a spray or fan of doubly charged particles (secondaries). The magnetic field separates the primaries and secondaries. Apertures to a detector limit the measurement of secondaries to those originating from spatially localized sample volumes.

B. Quantities measured

Quantities commonly measured with the HIBP are electron density fluctuations (normalized to local density), equilibrium electric potential, and electric potential fluctuations. The secondary ion current acquired as a function of time is governed by the equation

$$I_s = 2kI_0F_pF_s\sigma_{ion}l_{sv}n_e,$$

which depends on I_0 , the initial primary current σ_{ion} , the electron impact ionization cross section, the charge state (2) of the detected ion, l_{sv} , the sample volume length, n_e , the electron density at the sample volume, k , the detector secondary electron emission factor (1–10), and F_p and F_s , the primary and secondary beam attenuation factors. The secondary ion current is a direct measure of the fluctuating density in the

^{a)}Invited paper, published as part of the Proceedings of the 19th Topical Conference on High-Temperature Plasma Diagnostics, Monterey, California, May 2012.

^{b)}Author to whom correspondence should be addressed: drdemers@xanthotechnologies.com.

plasma, as

$$\tilde{n}_e / \langle n_e \rangle = \tilde{I}_s / \langle I_s \rangle,$$

where $\langle \rangle$ denotes a quantity average. The potential of the plasma at the measurement sample volume results in a difference between the energy of the injected ions (W_i) and detected ions. This potential, and its fluctuations, are given by

$$\phi = 2V_A(G + F \frac{i_U - i_L}{i_U + i_L}) - W_i, \quad \tilde{\phi} = 2V_A F \frac{i_U - i_L}{i_U + i_L},$$

where V_A is the analyzer voltage, i_U and i_L are the currents on the upper and lower plates of one detector, G is the analyzer gain, and F an off-line processing term. G and F depend on the entrance angle of the secondary ions into the analyzer, and were important considerations in the design of the HIBP for MST (as discussed in Sec. III).

II. THE HIBP ON A RFP

A. The Madison Symmetric Torus

The HIBP operation is well established in magnetic configurations such as those of a tokamak where the toroidal magnetic field dominates over other components and variations in the field from core to edge are smooth and helically unidirectional. The RFP fields, by contrast, have comparable toroidal and poloidal magnitudes, exhibit strong shear and the toroidal field reverses direction at the plasma edge as shown in Figure 1. The HIBP trajectories are therefore highly three dimensional, and have both toroidal and poloidal displacements. The poloidal component of the field is generated by the time-varying plasma current; this causes the beam trajectory to vary in time. Further, temporal topology and amplitude changes such as those associated with magnetic reconnection occur regularly during RFP operation. The resulting spatial and temporal characteristics of the beam are quite complex.

Other original challenges arising from the MST RFP include strong levels of UV radiation and elevated particle losses. These alter functionality of the HIBP electrostatic steering systems and generate high levels of noise on the detectors. Additional complications stem from the small diagnostic ports and the conducting vacuum vessel that has local magnetic field errors.

These complexities have necessitated the development of new operation and data analysis techniques. They include, but are not limited to, implementation of unique primary and secondary beamlines, adoption of alternative beam steering methods, development of higher precision accelerator and electrostatic steering system models, refinement of trajectory

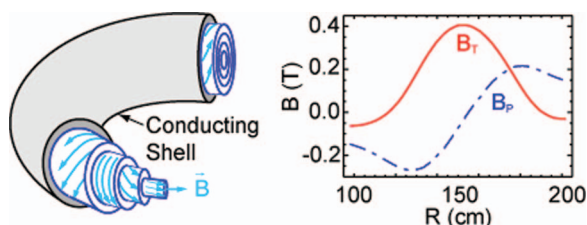


FIG. 1. The pitch of RFP magnetic field lines vary strongly with radius; the toroidal component reverses direction, hence “reversed field” pinch.

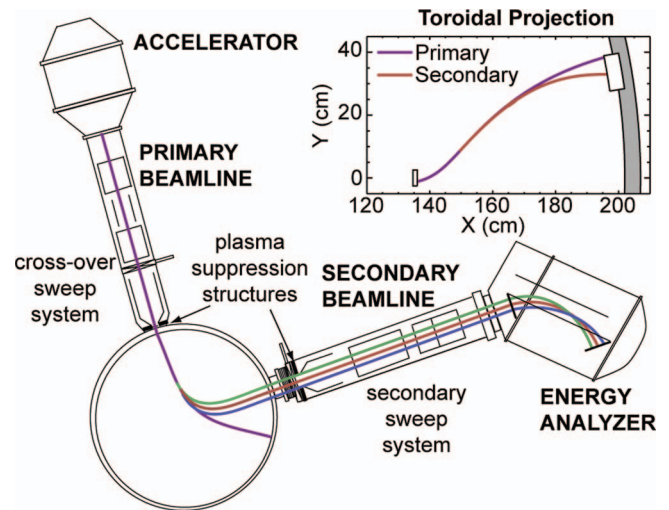


FIG. 2. The HIBP system installed on MST, with major components labeled. The 3D beam trajectory is shown.

calculations and sample volume modeling, establishment of stray particle and ultraviolet induced noise reduction methods, and formulation of alternative data analysis techniques. Sections III and IV discuss these innovative methods and the knowledge gained with this system.

B. The diagnostic setup

The main components of the HIBP system on MST, shown in Figure 2, are an accelerator, primary beamline, secondary beamline, and energy analyzer. A singly charged beam is produced, accelerated, and focused with a series of biased electrodes. The beam enters into the primary beamline and electrostatic steering system which alter its position and velocity. It travels through the injection port into the plasma, undergoes ionization, and produces a subset of secondaries that exit through the detection port and into the secondary beamline. The beam is directed to the apertures of the analyzer by another electrostatic steering system and deflected within the analyzer onto detectors. The beam is injected continuously and measurements are acquired as a function of time. The energy analyzer is a Proca and Green type electrostatic system^{2,3} having three apertures that enable simultaneous measurements from multiple plasma locations. There are three detectors, each comprised of four plates resulting in 12 signals that are digitized at 1MHz.

III. ADVANCES AND CHALLENGES

A. Primary crossover and secondary steering systems

As part of the initial development of the HIBP for MST, iterative simulations were performed to identify suitable beam energies and ions; electrostatic injection and detection systems were then designed around characteristics of the vacuum vessel and surrounding environment. The magnetic field structure, plasma cross section, as well as density and temperature profile are determining factors in the choice of

beam energy and ion. The major and minor radius of MST are $R = 1.5$ m and $a = 0.52$ m, and typical plasma parameters are $I_p < 600$ kA, $n_e < 2 \times 10^{13}$ cm $^{-3}$, and $T_e < 1.5$ keV. Measurements from the reversal surface toward the core are the priority. These criteria resulted in a HIBP design which produces, deflects, and detects singly charged sodium or potassium beams with energies up to 200 keV through ports separated by 10° toroidally and 86° poloidally.⁴ A toroidal displacement this large is uncommon but was chosen due to the deflection of the beam by the poloidal field.

The steering system designs were driven by the complicated 3D, temporal beam trajectories and the restricted diagnostic port diameters – just 5 and 11.4 cm. Frequently, the primary sweep system consists of two orthogonal pairs of plates used to steer the beam, with each pair having an effective sweep-point mid-way along their length.⁵ This design was found to be insufficient for such small ports, resulting in unique primary and secondary systems each designed to provide two-dimensional steering.⁶ The primary system is composed of four pairs of electrostatic plates arranged in a crossover⁷ orientation; two pairs deflect the beam in each direction, resulting in an effective sweep-point that is beyond the ends of the plates. This maximizes the angular range of deflection and results in increased probing coverage of the plasma. A sweep range of $\pm 20^\circ$ radially and $\pm 5^\circ$ toroidally, several times greater than other systems, is achieved through the 5 cm injection port.⁸

On many machines a secondary sweep system is not needed or has just one pair of plates. The MST required a system with three pairs because the secondaries produced in the RFP exit the machine with a range of angles that are incompatible with analyzer operation. The analyzer performs effectively and measurement errors (resulting from G and F) are minimized when the angle of the beam into the analyzer is near 0° in the direction parallel to the apertures and less than $\pm 5^\circ$ in direction perpendicular to them.⁹ The secondary sweep system was designed to reduce the entrance angle of the beam into the analyzer from $\pm 17^\circ$ to $\pm 3^\circ$ in the perpendicular and from $\pm 5^\circ$ to 0° in the parallel direction. The bias voltage of each plate is controlled by one of fourteen 4–20 kV high voltage amplifiers with bandwidth up to 40 kHz.

B. Finite-sized beam modeling

The trajectory simulations used to model beam ion paths from the accelerator to the analyzer on most HIBPs (installed on devices in the United States) have been modest. The MST HIBP requires more detailed simulations due to the small diagnostic ports, the primary and secondary sweep systems, the temporal 3D beam trajectory, and magnetic shear which result in complex modifications to the paths of the beam ions. We have developed a finite-sized beam model, comprised of many beamlets (or point-sized beams) distributed throughout a circular cross section, to characterize the beam along its trajectory. A 21-point model provides a reasonable balance between computation time and resolution. It allows us to assess effects of the electrostatic systems, EM fields, and scrapeoff

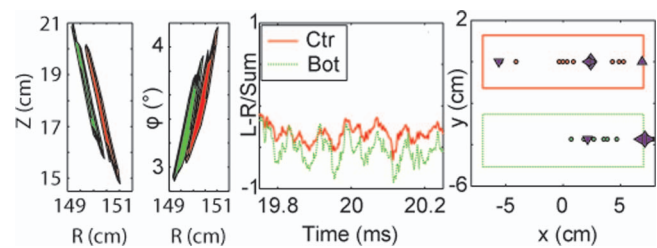


FIG. 3. A finite-sized beam model is used to characterize the sample volumes. It also demonstrates agreement between simulated and measured distributions of secondary ion current at the detector.

(due to interaction with structures), and characterize sample volumes and detected ion current.

1. Sample volume characterization

A mapping of the beamlets that impact the entrance apertures of the analyzer to their ionization location in the plasma determine the sample volume locations, orientations, and shapes. The sawtooth cycle and actively driven improved confinement (IC) periods consist of temporal evolution of the magnetic field^{10,11} which alter the trajectories. The movement may cause scrapeoff and change the characteristics of one or more sample volumes – issues that can be examined with the model. Additionally, the temporal magnetic field causes the sample volumes to undergo 3D motion as a function of time.¹² Common displacements over the course of an IC period are $\Delta x = 0.5$ cm, $\Delta y = 0.8$ cm, and $\Delta z = 1.3$ cm. This leads to a total radial displacement $\Delta \rho = 1.6$ cm.

2. Fan angle

The utility of the model may be further demonstrated through a study of the impact of RFP magnetic field shear on the secondary ion fan. Simulations indicate that sample volumes near the core produce a fan that is nearly perpendicular to the apertures of the analyzer (the desired orientation), whereas those near the edge produce one nearly parallel. The rotation of the spray occurs because the toroidal field dominates in the interior and the poloidal field near the edge. Figure 3 shows (a slice of) the fan from a sample volume near $r/a = 0.4$ puncturing the aperture plane; it deviates from normal but is not disabling. A comparison with experimental data indicates that the model prediction is consistent with the distribution of current measured on the right and left halves of two detectors as shown in Figure 3. Toroidal translation of the secondary beamline by $\pm 10^\circ$ (to accommodate beam exit angles) with 90° of analyzer rotation (to orient the fan perpendicular to the apertures) would enable full profile measurements and minimize instrumental errors; hardware does not currently allow this. Magnetic configurations where the toroidal field dominates over other field components result in a fan that is largely normal to the apertures.

C. Stray particle and secondary electron mitigation

The adverse impact of stray particles and radiation from MST on the HIBP has exceeded all past installation

experiences. The total particle plus radiated power from the plasma is on the order of 1.7–2.0 MW.¹³ High levels of flux into the beamlines during plasma startup, ramp-down, and magnetic reconnection make operation challenging. Plasma particles and secondary electrons (produced by UV photons striking metal beamline components) appear as a current load on the amplifiers driving the sweep plates and cause a voltage drop when the current draw exceeds the amplifier limit. This process has a detrimental effect on sweep plate operation and subsequent steering of the beam.

The port size restrictions on MST necessitated sweep systems that are closer to the plasma than in most other diagnostic installations. The leading edges of the plates in the primary and secondary beamline are just 10 and 25 cm from the plasma, respectively. Despite the small port sizes, the passage of particles and radiation is large. To fully understand the dynamics, the ion optics software SIMION (Ref. 14) was used to simulate the plates, electric fields (which range from 2 to 8 kV/cm during operation), surrounding chambers, and particle motions. Electrons liberated by UV travel from the chamber walls and negatively biased sweep plates to the positively biased ones. Large current loads cause a voltage lapse which results in a misdirected beam and ultimately a loss of detected secondary ion signals.

These issues prompted development of permanent magnet plasma suppression structures which are strong enough (magnetic fields as large as 1.7 kG) to prevent plasma particles from entering the beamline while allowing the HIBP ions to pass. The magnetic fields are perpendicular to the general motion of the particles and produced with nickel plated NdFeB magnets lining soft-iron flux keepers. A complete discussion of these structures was published previously.¹⁵ They are effective at reducing the plasma leakage to minimal levels; the remaining load appears to be due to UV.

Conventional sweep operation applies equal and opposite voltages on parallel pairs of plates. The performance of the amplifiers controlling the plates nearest to MST varies with discharge conditions, but in general those driving plates to a positive bias regularly saturate, whereas those driving plates to a negative bias operate as desired (though they may momentarily overload during reconnection events). Our solution to deal with this current load induced by UV is to ground the plates normally biased positive and drive only those normally biased negative. Doubling the voltage of the negatively biased plate largely restores the electric field and effective sweep angle. While this technique is unconventional, it is effective during intervals with moderate UV flux, but during strong radiation there remain periods when the voltage still drops due to amplifier limitations of ± 20 mA. We quantified the current needed to maintain voltage during most plasma conditions and subsequently installed amplifiers capable of ± 80 mA.

D. High precision electrostatic and magnetic modeling

Since the ion beam is highly sensitive to electric and magnetic fields, small inaccuracies in modeled fields lead to differences between actual and simulated trajectories which are accentuated over long distances. The use of primary and

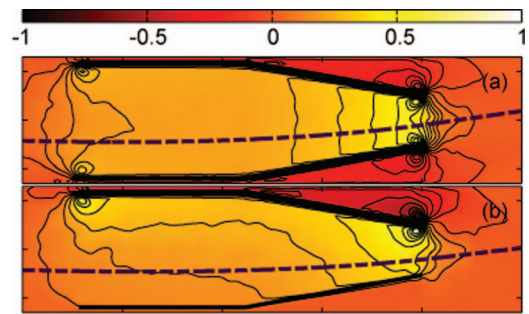


FIG. 4. This finite element method model demonstrates electric field contours are (a) symmetric during equal and opposite plate biasing and (b) asymmetric during single plate biasing.

secondary beamlines and generation of a significant fraction of the magnetic field by the plasma amplifies this issue in the RFP. Elements of the MST system that are modeled include primary and secondary sweep plate fields and permanent magnet plasma suppression structures; magnetic field errors at the ports; and the plasma EM fields. An immense component of HIBP operation on the RFP is accurate and iterative modeling; interpretation of data and inference of measurements depend critically on these efforts.

1. HIBP electric field modeling

The electrostatic model used to design the steering systems for MST works well for calculating electric fields when traditional equal and opposite plate biases are applied. However, when one plate is grounded and a single plate biased (as is necessary), there is an asymmetry in the electric field which the model cannot accurately simulate. This has motivated the development of a finite-element model of the sweep systems that finds the solution to Laplace's equation with boundary conditions given by the bias potentials of the sweep plates. This numerical solution more accurately computes the non-uniformity and fringe fields in the beamlines. Figure 4(a) shows that the electric field contours are symmetric with traditional biasing, whereas Fig. 4(b) depicts the asymmetry in the single plate method. The beam (dashed violet line) travels (left to right during experimental operation) and into an electric field which is substantially different for single plate bias than originally specified. A deviation between the intended and resultant beam angles and positions can be seen on the RHS of the figure. Similar results are realized when the model is applied to the secondary steering system.

2. Port field error and magnet structure modeling

The magnetic field errors produced by the ports and those produced by the plasma suppression structures are rather unique to the HIBP on MST, because in other magnetic confinement configurations they are negligible or absent. Each of these fields deflects the beam and has significant impact on the trajectory.¹⁶ The fields produced by the permanent magnet plasma suppression structures¹⁵ are static. They are modeled using a series of square cross-section current loops normalized to measurements. We have also developed an analytic solution for the magnetic field errors produced by ports in the

MST conducting vacuum vessel.¹⁷ It is used to model the field errors caused by image currents diverting around the injection and detection ports. Comparisons between measured and simulated ion current distributions on the detectors suggest agreement improves when these models are included. Sample volume localization, which is critical to determination of the radial electric field, is also improved.

E. Discrimination of reconstructed magnetic fields

The magnetic field profiles used in HIBP simulations are obtained through Grad-Shafranov equilibrium reconstruction produced by MSTFit. Accuracy of the reconstruction depends on the model and the diagnostic data that constrain it. Since the trajectory of the ion beam is (largely) determined by the magnetic field and sensitive to small changes in magnetic equilibrium it contributes additional unique information useful in constraining MSTFit.^{18,19}

During HIBP experimental operation, the location and velocity of the primary beam as it enters the plasma are well known. While those of the secondary ions are not, they are restricted to a $\pm 3^\circ$ toroidal exit angle by the secondary beamline hardware. The distribution of the secondary ion current on two detectors is also known. The HIBP trajectory simulation code can be operated using this information and multiple reasonable magnetic equilibria produced by MSTFit. The equilibrium and resultant beam trajectories that produce a simulated secondary ion current distribution that best matches experimental data likely indicate the most plausible magnetic equilibrium.

F. Data and analysis

The first data acquired from MST with the HIBP had relatively weak secondary current levels (20–40 nA) and strong noise levels (due to UV).²⁰ The detected ion current (I_s) produced from a reasonable injected beam current was low and due largely to the quantities n_e and l_{sv} . The nominal electron density in MST is 3–6 times lower than in many other machines, and the sample volume dimension l_{sv} can also be smaller. Maximizing n_e does not linearly increase I_s since the attenuation of the primary and secondary beams will also increase (decreasing F_p and F_s). The quantity most readily increased is the injected ion current I_0 since beam production is a function of accelerator operation.

The accelerator structure and the methods by which it is operated determine the beam characteristics and ion optics. Thus, the system was modeled to ascertain more efficient methods of operation.²¹ Experiments in which we applied the parameters identified in simulation to hardware confirm significant improvements; primary currents are reliably $\sim 100 \mu\text{A}$ and beam diameters $\sim 1 \text{ cm}$.

Control systems of many HIBPs are near the diagnostic because discharges are reproducible and static setting are sufficient. This mode of operation is inadequate for the RFP and the control systems were redesigned and relocated into the main control room. The beam is now manually refocused and pulsed prior to each discharge resulting in further extraction and focus improvements. The measured secondary ion current

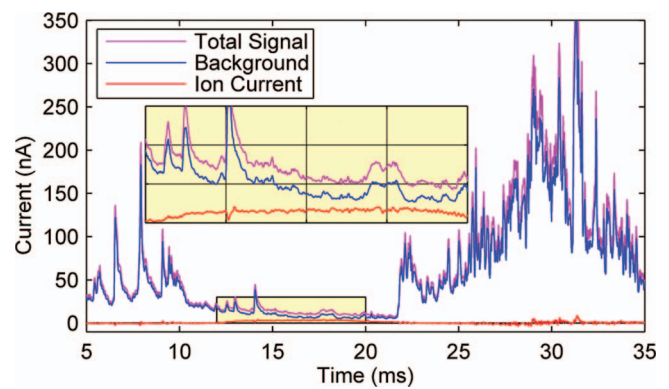


FIG. 5. Application of the *background* noise subtraction method to a *total signal* (comprised of ion current and UV noise) reveals the secondary *ion current* (from 12 to 20 ms) and reduces the UV current to near zero.

is repeatedly 60–250 nA (up to a factor of six times larger than measured previously under similar conditions).

1. UV noise mitigation

High levels of UV flux shining from the MST plasma into the analyzer and onto the detectors cause the production of secondary electrons (which have the same signature as an ion.)¹⁵ The resultant UV induced detector current exceeds 100 nA during plasma formation and reconnection events, yet falls below 20 nA during IC periods. When inferring fluctuation magnitudes from measurements with low to moderate secondary signals, UV induced current can cause errors.²²

This motivated development of a method to remove the UV noise from data. The noise on each plate is observed to be nearly identical with only slight differences in magnitude. Measurements are now taken with one of the 3 analyzer apertures closed; the corresponding (*background*) detector signal, shown in Figure 5, is then only UV induced current. Multiple discharges without an ion beam are used to ascertain unique noise calibration factors for each detector plate relative to the background plates. Subsequent measurements subtract appropriately scaled background noise from each plate of the active detectors; the *total signal* shown in Fig. 5 is a combination of both secondary ion and UV induced current. Application of the noise subtraction method reveals the secondary *ion current* (from ~ 12 –20 ms) and effectively reduces the UV noise current to zero before and after this period. Calculated density and potential fluctuation levels have error bars that scale inversely with signal level. Background subtraction reduces error bars on weak (20 nA) signals from $\sim \pm 100\%$ to $\pm 10\%$; for signal levels $> 100 \text{ nA}$ the method reduces the effect of UV noise below that of other sources.

Data acquired with the HIBP on MST are often a combination of plasma and instrumental features. This compelled identification of characteristics associated with instrumental effects and the critical screening of all data for such features prior to routine processing. Improved control of the ion beam, rotation and translation of the analyzer, and refinement of diagnostic hardware will reduce instrumental effects.

The diagnostic advances achieved on the MST are enabling measurements from the RFP interior. The fluctuations in electron density and potential measured with the HIBP are

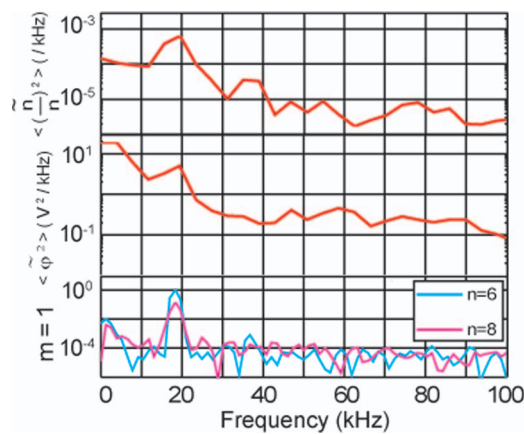


FIG. 6. Low frequency fluctuation power peaks of \tilde{n}/n and $\tilde{\phi}$, correlate largely with those of the dominant tearing modes.

broadband with most power below 300 kHz, as shown in Fig. 6. The low frequency fluctuation power peaks correlate largely with those of the dominant ($m = 1$, $n = 6$) tearing mode. Correlation between magnetic modes and electrostatic fluctuations is also observed by other experiments.²³ These data are acquired from a sample volume near the $m = 1$, $n = 6$ –8 rational surfaces in the vicinity of $r/a = 0.4$.

IV. SUMMARY AND OUTLOOK

Many aspects of the RFP present original challenges to HIBP operation and the inference of plasma quantities. Characteristics of the machine, confining magnetic field, and plasma contribute to a number of these issues. These complexities have demanded development of new components, operation and techniques. They include implementation of primary and secondary beamlines, adoption of alternative beam steering methods, development of higher precision accelerator and electrostatic system models, refinement of trajectory calculations and sample volume modeling, establishment of stray particle and ultraviolet induced noise reduction methods, and formulation of alternative data analysis techniques.

The advances realized with the HIBP on the RFP are likely to facilitate future operation on alternative confinement, large scale or high power devices. Each innovative method is of value in several scenarios. For example, the capability to acquire measurements during time-varying equilibria will translate to operation in tokamaks during sawtooth oscillations, disruptions, and edge localized modes (ELMs), and in spherical tokamaks with coaxial helicity injection. Operation on a spheromak may also benefit from the techniques to acquire measurements in a magnetic field with strong shear. The innovative methods developed to operate in strongly radiative environments will be of broad value to the diagnosis of regions such as edges and divertors, and have application on larger tokamaks in which ELMs and disruptions might be present.

ACKNOWLEDGMENTS

The authors would like to thank the team at the Madison Symmetric Torus for their support of this work. We also recognize the substantial contributions of P.M. Schoch, J. Schatz, J. Lei, U. Shah, X. Zhang, and X. Chen.

This material is based upon work supported by the U.S. Department of Energy (DOE) under Award No. DE-SC0006077. Neither the United States Government nor any agency thereof, nor any of their employees, makes any warranty, express or implied, or assumes any legal liability or responsibility for the accuracy, completeness, or usefulness of any information, apparatus, product, or process disclosed, or represents that its use would not infringe privately owned rights. Reference herein to any specific commercial product, process, or service by trade name, trademark, manufacturer, or otherwise does not necessarily constitute or imply its endorsement, recommendation, or favoring by the U.S. Government or any agency thereof. The views and opinions of authors expressed herein do not necessarily state or reflect those of the U.S. Government or any agency thereof.

- ¹T. P. Crowley, *IEEE Trans. Plasma Sci.* **22**(4), 291 (1994).
- ²T. S. Green and G. A. Proca, *Rev. Sci. Instrum.* **41**, 1409 (1970).
- ³T. S. Green and G. A. Proca, *Rev. Sci. Instrum.* **41**, 1778 (1970).
- ⁴U. Shah, K. A. Connor, J. Lei, P. M. Schoch, T. P. Crowley, J. G. Schatz, and Y. Dong, *Rev. Sci. Instrum.* **70**, 963 (1999).
- ⁵J. R. Goyer, K. A. Connor, R. L. Hickok, and L. Solensten, *IEEE Trans. Plasma Sci.* **22**(4), 403 (1994).
- ⁶J. Lei, T. P. Crowley, U. Shah, P. M. Schoch, K. A. Connor, and J. Schatz, *Rev. Sci. Instrum.* **70**, 967 (1999).
- ⁷“Crossover” refers to parallel pairs of sweep-plates that steer the beam in alternate directions to maximize the angular deflection of the ion beam.
- ⁸J. Lei, U. Shah, D. R. Demers, K. A. Connor, and P. M. Schoch, *Rev. Sci. Instrum.* **72**, 564 (2001).
- ⁹L. Solensten and K. A. Connor, *Rev. Sci. Instrum.* **58**, 516 (1986).
- ¹⁰J. S. Sarff, N. E. Lanier, S. C. Prager, and M. R. Stoneking, *Phys. Rev. Lett.* **78**, 62 (1997).
- ¹¹B. E. Chapman *et al.*, *Phys. Plasmas* **9**, 2061 (2002).
- ¹²D. R. Demers, X. Chen, P. M. Schoch, and P. J. Fimognari, *Rev. Sci. Instrum.* **81**, 10E109 (2010).
- ¹³N. E. Lanier, Ph.D. dissertation, University of Wisconsin-Madison, 1999.
- ¹⁴D. A. Dahl, *International Journal of Mass Spectrometry* **200**, 3 (2000).
- ¹⁵D. R. Demers, K. A. Connor, J. Lei, P. M. Schoch, and U. Shah, *Rev. Sci. Instrum.* **72**, 568 (2001).
- ¹⁶P. J. Fimognari, D. R. Demers, B. E. Chapman, X. Chen, D. J. Den Hartog, G. Fiksel, and J. S. Sarff, *Proceedings of the 36th EPS Conference on Plasma Physics* (European Physical Society, Sofia, 2009), Vol. 33E, p. 1.175.
- ¹⁷P. J. Fimognari, A. F. Almagri, J. K. Anderson, D. R. Demers, J. S. Sarff, V. Tangri, and J. Waksman, *Plasma Phys. Controlled Fusion* **52**, 095002 (2010).
- ¹⁸D. R. Demers, P. M. Schoch, R. J. Radke, J. K. Anderson, D. Craig, and D. J. Den Hartog, *Rev. Sci. Instrum.* **74**, 2103 (2003).
- ¹⁹C. Ling, K. A. Connor, D. R. Demers, R. J. Radke, and P. M. Schoch, *Rev. Sci. Instrum.* **78**, 113505 (2007).
- ²⁰D. R. Demers, J. Lei, U. Shah, P. M. Schoch, K. A. Connor, T. P. Crowley, J. G. Schatz, J. K. Anderson, and J. S. Sarff, *Czech. J. Phys.* **51**(10), 1065 (2001).
- ²¹D. R. Demers, K. A. Connor, P. M. Schoch, R. J. Radke, J. K. Anderson, D. Craig, and D. J. Den Hartog, *Rev. Sci. Instrum.* **75**, 4187 (2004).
- ²²X. Zhang, J. Lei, K. A. Connor, D. R. Demers, P. M. Schoch, and U. Shah, *Rev. Sci. Instrum.* **75**, 3502 (2004).
- ²³T. Ido *et al.*, *Nucl. Fusion* **51**, 073046 (2011).